Impact of SO2 injection profiles on simulated volcanic forcing for the Sarychev 2009 eruptions - investigating the importance of using high vertical resolution methods when compiling SO2 data

Emma Axebrink[1], Moa K. Sporre[1], and Johan Friberg[1]

[1]Department of Physics, Lund University, Lund 22100 Sweden

Correspondence: Johan Friberg (johan.friberg@fysik.lu.se)

Abstract. Aerosols from volcanic eruptions impact our climate by influencing the Earth's radiative balance. The degree of their climate impact is determined by the location and injection altitude of the volcanic SO_2. To investigate the importance of utilizing correct injection altitudes we ran climate simulations of the June 2009 Sarychev eruptions with three SO2 datasets, in the Community Earth System Model Version 2 (CESM2) Whole Atmosphere Community Climate Model Version 6 (WACCM6).

We have compared simulations with WACCM's default $1 \, \mathrm{km}$ vertically resolved dataset M16 with our two $200 \, \mathrm{m}$ vertically resolved datasets, S21-3D and S21-1D. The S21-3D is distributed over a large area (30 latitudes and 120 longitudes), whereas S21-1D releases all SO_2 in one latitude and longitude grid-box, mimicking the default dataset M16.

For S21-1D and S21-3D, 95% of the SO_2 was injected into the stratosphere, whereas M16 injected only 75% to the stratosphere. This difference is due to the different vertical distribution and resolution of SO_2 in the datasets. The larger portion of SO_2 injected into the stratosphere for the S21 datasets leads to more than twice as high sulfate aerosol load in the stratosphere for the S21-3D simulation compared to the M16 simulation during more than 8 months. The temporal evolution in AOD from two of our simulations, S21-3D and S21-1D, follows the observations from the space-borne lidar instrument CALIOP closely, while the AOD in the M16 simulation is substantially lower. This indicates that the injection altitude and vertical resolution of the injected volcanic SO_2 substantially impact the model's ability to correctly simulate the climate impact from volcanic eruptions.

The S21-3D dataset with the high vertical and horizontal resolution resulted in global volcanic forcing of -0.24 $\mathrm{W/m^2}$ during the first year after the eruptions, compared with only -0.11 $\mathrm{W/m^2}$ for M16. Hence, our study highlights the importance of the vertical distribution of SO_2 injections in simulations of volcanic climate impact, and calls for a re-evaluation of further volcanic eruptions.

1 Introduction

Aerosols impact our climate by influencing the Earth's radiative balance – directly by scattering and absorbing solar radiation and indirectly via influencing cloud properties. These effects result in a net cooling effect on the climate. Aerosol emissions from fossil fuel combustion have counteracted some of the warming effects of anthropogenic greenhouse gases (Hansen et al., 2023). However, aerosols' climate impact is still a subject of great uncertainty (IPCC, 2021). It is important to understand natural sources of aerosols in order to better understand how humans affect the climate via emissions of greenhouse gases (Myhre et al., 2013; Robock, 2000).

Explosive volcanic eruptions that inject effluents into the stratosphere are a natural source of the particle forming gas SO_2, and can have a large impact on the climate (Robock, 2000). The volcanic SO_2 is converted into sulfuric acid forming particulate matter, which can remain in the stratosphere for months or years inducing long-term negative radiative forcing by scattering incoming solar radiation (Sigl et al., 2015). The aerosol is eventually removed from the stratosphere in the extratropics when the air is transported to the troposphere (Sigl et al., 2015; Gettelman et al., 2011; Appenzeller et al., 1996; Solomon et al., 2011). The severity of the climate impact is determined by the explosivity of the eruption, the mass of the stratospherically injected SO_2, the injection altitude, and the location of the volcano (Robock, 2000; Kremser et al., 2016).

Volcanic eruptions have from time to time substantially cooled the Earth's climate (Sigl et al., 2015). The 1991 Mt. Pinatubo eruption is the latest eruption where a large amount of SO_2 reached high up into the atmosphere and lowered the global averaged surface temperature by several tenths of a degree Celsius (Kremser et al., 2016). Apart from such large size eruptions, less explosive eruptions add to variability in the stratospheric aerosol load and cause substantial effect on the climate (Andersson et al., 2015; Vernier et al., 2011; Friberg et al., 2018), including the Sarychev eruptions in June 2009 simulated in the present study.

The vertical distribution of SO_2 from a volcanic eruption is crucial information, since the altitude determines the residence time of the aerosols (Andersson et al., 2015; Friberg et al., 2018; Kremser et al., 2016; Robock, 2000). Aerosols in the stratosphere can have a residence time of several years whereas tropospheric aerosols have a residence time of weeks or less (Kremser et al., 2016). Stratospheric aerosols thus have a prolonged climate impact compared to tropospheric aerosols (Robock, 2000; Deshler, 2008). For a volcanic eruption to affect the climate more long-term, the emitted sulfur needs to reach the stratosphere, i.e. be an explosive volcanic eruption. Less explosive eruptions often position the SO_2 in the vicinity of the tropopause. To estimate the climate impact of such eruptions, it is of particular importance to place the SO_2 at the correct altitude (Schmidt et al., 2018).

To investigate volcanic eruptions and their climate impact, global Earth System Models (ESMs) can be utilized. Global modelers often use satellite-based observations of volcanic SO_2 as input when simulating the volcanic impact on the stratosphere and climate. SO_2 satellite instruments are passive sensors and therefore lack direct vertical measurements. The altitude of the SO_2 clouds are therefore indirectly estimated resulting in coarse vertical resolution with substantial uncertainties. Clarisse et al. (2014) showed that IASI can provide SO_2 data with vertical resolution down to ~2 km, and MIPAS has a vertical resolution of 3-5 km (Höpfner et al., 2015). This is on the order of one magnitude coarser than typical SO_2 layers from the June 2009

Sarychev eruptions (Sandvik et al., 2021). In Sandvik et al. (2021) we combined passive satellite measurements from the AIRS (Atmospheric Infrared Sounder) satellite instrument with the active satellite sensor CALIOP (Cloud-Aerosol Lidar with Orthogonal Polarization) and created an SO_2 inventory with approximately 60 meter vertical resolution. With this method we create a 3D dataset where we provide altitude information for different SO_2 layers from the same eruption emitted at different times and altitudes.

ESM simulations of explosive volcanic eruptions' climate impact are generally run with vertical SO_2 profiles released above, or in the vicinity of, the volcano site (Timmreck et al., 2018). This requires that the meteorology and tropopause height are simulated correctly in order to represent the transport of the volcanic aerosol during the first few days after the eruption. Small errors in horizontal or vertical transport may cause errors in the evolution of the SO_2 distribution (Tilmes et al., 2023) and transport of the formed sulfate particles, and ultimately in the resulting climate impact. Using a 3D dataset retrieved a few days after the eruption could reduce such uncertainties.

To investigate the importance of utilizing a high vertically and horizontally resolved volcanic SO_2 emission dataset, we used the SO_2 dataset of Sandvik et al. (2021) as input to an ESM. We have modeled the eruptions of Sarychev Peak in June 2009. This volcano is located in the Northern Hemisphere (NH) at the center of the Kuril islands (48.092°N 153.20°E). This case is considered to be a complex series of volcanic eruptions since it erupted for several days and injected SO_2 over a wide range of altitudes. The duration of the eruption was from the 11th to the 16th of June, spreading SO_2 from 11-19 km altitude. The total mass of SO_2 emitted from the eruptions has been reported to range from 0.6 to 1.2 Tg (Carboni et al., 2016; Haywood et al., 2010).

In this study, we ran three simulations with different SO_2 emission datasets with the Community Earth System Model version 2 (CESM2.1), Whole Atmosphere Community Climate Model (WACCM6). The first is WACCM's default volcanic SO_2 single column dataset with an assumed vertical profile, at 1 km resolution (Mills et al., 2016). The second is a dataset at 200 m vertical resolution where the SO_2 is distributed over a wide geographical region representing the initial spread of SO_2 based on Sandvik et al. (2021). The third dataset is a hybrid between the first two and constitutes a single column dataset at 200 m vertical resolution compiled from Sandvik et al. (2021). All simulations are evaluated by comparison to aerosol observations from the satellite sensor CALIOP.

2 Method

In this section, we describe the SO_2 datasets used in the Earth system model, how they were created, and the differences between them. A brief model description is also included in this section and a description of the satellite dataset we compare the model simulations to.

2.1 SO_2 data

We have inserted the SO_2 dataset of the 2009 Sarychev Peak eruption described in Sandvik et al. (2021). It was compiled by combining horizontally resolved SO_2 data from the satellite-instrument Atmospheric Infrared Sounder (AIRS) aboard the satellite Aqua, with the vertical aerosol profiles from the satellite-instrument CALIOP. The SO_2 and aerosol observed from these instruments were assumed to be co-located and therefore have the same height profile. The aerosol data from CALIOP (at 60 m resolution) was coupled to the SO_2 data from AIRS using the dispersion model FLEXPART (FLEXible PARTicle dispersion model), enabling retrieval of vertical profiles of the SO_2 layers with a high resolution (Sandvik et al., 2021). For a more detailed description of the method used to obtain this dataset we refer to Sandvik et al. (2021)

The Sarychev Peak erupted multiple times over several days, starting on the 11 of June and continuing for 5 days. However, most of the SO_2 was emitted on the 15 of June (Rybin et al., 2011). The dataset from Sandvik et al. (2021) contains data from AIRS swaths around midnight between the 18 and 19 of June. The (Sandvik et al., 2021) 3D dataset has a vertical resolution of 1 K in potential temperature, corresponding to 61 ± 56 m or 1.8 ± 2.9 mbar. In this study, we ran the model with a re-gridded version of this dataset with a vertical resolution of 200 m and a horizontal resolution of $0.95°$ latitude $\times$ $1.25°$ longitude.

2.2 Model description

Simulations were run with the Specified Dynamic (SD) version of the WACCM6 (Gettelman et al., 2019). WACCM6 is an extension of the Community Atmosphere Model version 6 (CAM6), and part of the Community Earth System Model Version 2 (CESM2.1) (Danabasoglu et al., 2020). WACCM6 is a global high-top atmospheric model, spanning from the surface to the thermosphere. The WACCM6-SD has a top altitude of 140 km with 88 levels. We ran the model with a horizontal resolution of $0.95°$ latitude $\times$ $1.25°$ longitude with an active atmosphere and land, but prescribed sea-surface temperatures (SSTs) and sea-ice concentrations (Gettelman et al., 2019).

WACCM6 includes advanced atmospheric chemistry in the troposphere, stratosphere, mesosphere, and lower thermosphere (TSMLT). The chemistry includes 231 solution species, and the following chemical reactions; 150 photolysis reactions, 403 gas-phase reactions, 13 tropospheric, and 17 stratospheric heterogeneous reactions. For the stratospheric reactions, three types of aerosol particles are included, sulfate, nitric acid trihydrate, and water-ice (Gettelman et al., 2019). Sulfates in the stratosphere are produced by the chemical oxidation of SO_2 by the OH radical. The sulfate will then, via intermediate steps, produce H_2SO_4 gas (Liu et al., 2012; Mills et al., 2017). The H_2SO_4 gas can either condensate on existing particles or form new particles through binary H_2SO_4-H_2O nucleation (Vehkamäki et al., 2002, 2013). The newly formed particles are added to the Aitken mode after growth according to the parameterization from Kerminen and Kulmala (2002).

Table 1. Properties for the three input SO$_2$ datasets.

Dataset name	S21-3D	S21-1D	M16
Vertical resolution	200m	200m	1km
Horizontal resolution	0.95° × 1.25°	single column	single column
Vertical distribution	11 - 19 km	11 - 19 km	11 - 15 km
Release date	19th of June	15 - 16th of June	15 - 16th of June
SO$_2$	1.09 Tg	1.09 Tg	1.2 Tg

WACCM6 utilizes the Modal Aerosol Model, four-mode version, (MAM4) as standard. This includes Aitken, accumulation, coarse, and a primary carbon mode (Liu et al., 2016). MAM4 in WACCM6 includes modifications of the aerosol code to better represent aerosol processes in the stratosphere (Mills et al., 2016). The MAM4 gas-aerosol exchange module treats stratospheric sulfate as aqueous SO$_4^=$. The H$_2$SO$_4$ equilibrium vapor pressure treats condensation and evaporation of H$_2$SO$_4$ in the stratosphere to allow for shrinkage and growth between the accumulation and coarse mode (Mills et al., 2016).

The Specified Dynamic (SD) version (WACCM6-SD) allows the simulations to be nudged. We have nudged with Modern-Era Retrospective analysis for Research and Applications, version 2 (MERRA2) from the surface to 50 km with a relaxation between 50 and 60 km and no nudging above 60 km. The horizontal winds and surface pressure were nudged while temperature nudging was not used.

2.3 Simulation description

Three different simulations, referred to as S21-3D, S21-1D, and M16, were run over the period of January 2009 to December 2010 to investigate the eruption of Sarychev Peak in 2009 with different vertical and horizontal resolutions of SO$_2$ datasets as input. The differences between the input datasets for the simulations are summed up in Table 1 with further details below.

The first simulation, M16, was run with the default SO$_2$ dataset, Volcanic Emissions for Earth System Models, version 3.11 (Neely and Schmidt, 2016, VolcanEESM), for the Sarychev eruption from WACCM6. For 2009 and 2010, all eruptions except Sarychev's were removed. M16 is a single column (1D) emission dataset with a vertical resolution of 1 km. 0.6 Tg of SO$_2$ was released on two occasions, 15 and 16 of June, e.g. a total of 1.2 Tg. The SO$_2$ was released over a time period of 6 hours, starting at 12:00 UTC and ending at 18:00 UTC. This is the same approach that has been used in previous studies of this eruption using WACCM (Neely and Schmidt, 2016; Mills et al., 2016).

The second simulation, S21-3D, was run with a volcanic SO$_2$ dataset for the Sarychev eruption and was created from the work of Sandvik et al. (2021). This dataset has a vertical resolution of 200 m and a horizontal resolution of 0.95° latitude × 1.25° longitude. The SO$_2$ is vertically distributed between 10 and 19 km and horizontally between the longitudes 130°E and 130°W, Figure 1. The S21-3D dataset releases all 1.09 Tg SO$_2$ over a time period of two hours, starting on the 19th of

June at 00:30 UTC and ending at 02:30 UTC. The SO2 was released at the times that the AIRS instrument recorded the SO2 concentration.

The third simulation, S21-1D, utilizes the dataset of the first simulation but with the horizontal distribution summed up, making the dataset into a single column (1D) emission file. The dataset has the same vertical resolution of 200 m as the S21-3D dataset. The SO_2 is released on the 15 and 16 of June over a time period of 6 hours, starting at 12:00 UTC and ending at 18:00 UTC, i.e. the same emission times as in the M16 simulation. The total amount released is the same as for S21-3D, 1.09 Tg. This dataset was created to mimic the M16 dataset, described above. When the SO_2 is emitted in the model it is interpolated to the model grid which is the same for all simulations.

The first five months of the simulations were run without any volcanic forcing and served as a spin-up. The three simulations, S21-3D, S21-1D, and M16, were run as branches from the spin-up simulation for an additional 19 months, from the first of June 2009 to the last of December 2010. We have also run a simulation without any volcanic emissions (No-Volc).

The differences in the vertical and horizontal profile for the three SO_2 emission datasets are shown in Fig. 1. S21-3D and S21-1D have identical vertical profiles as shown in Fig. 1a. We can clearly see that much of the SO_2 in the S21-3D and S21-1D is located at a higher altitude compared to the default dataset M16. S21-3D and S21-1D are also more spread vertically compared with M16. Figure 1b shows the horizontal distribution of the SO_2 input dataset in simulation S21-3D. The red triangle marks the location for Sarychev Peak and is the location where M16 and S21-1D release the SO_2. The several eruptions from the Sarychev peak during these days reached different altitudes, leading to the broad horizontal distribution seen in Fig 1 b-d. The SO_2 layers located around 140°W was injected at higher altitude and has the majority of the SO_2 mass located at around 15 km. The SO_2 layers located around 130°E is positioned at lower altitudes with the majority of the mass at approximately 12-13 km altitude. The Eastern and Western SO_2 layers were transported in very different directions relative to the volcano clearly displaying the complexity of this eruption.

2.4   Aerosol data - satellite-derived aerosol extinction coefficients

The model simulations were compared with aerosol extinction data compiled from satellite observations retrieved by the space-borne lidar CALIOP. The sensor acquired data at 532 and 1064 nm, and had a polarization filter to retrieve depolarization data at 532 nm. We used nighttime data in the latest version of the lowest level available, i.e. the Level 1b v4-51 (Product CAL_LID_L1-Standard-V4-51). Data were screened for ice clouds in the lowest 3 km of the stratosphere using depolarization ratios, and polar stratospheric cloud data were removed using a temperature threshold of 195 K outside 60°S - 60°N (see Friberg et al. (2018), Martinsson et al. (2022) and Friberg et al. (2023) for details). Backscattering coefficients were computed by correcting for light attenuation by particles and molecules (including ozone) throughout the stratosphere (Friberg et al., 2018; Martinsson et al., 2022; Friberg et al., 2023). Extinction coefficients were computed using a lidar ratio of 50 sr, i.e. a typical extinction to backscattering value for volcanic aerosol (Jäger and Deshler, 2002, 2003).
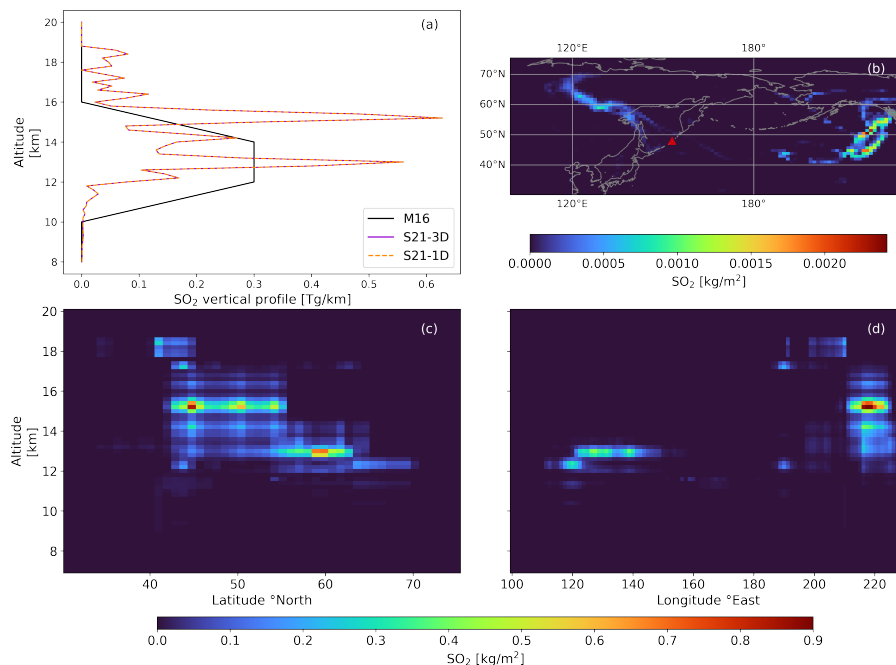
Figure 1. (a) Vertical SO$_2$ profiles for the three input datasets of each simulation. The vertical profile for M16 and S21-1D is the summed total injection for the eruption on the 15th and the 16th of June, whereas the vertical profile for S21-3D is the total injection on the 19th of June. **(b)** Vertically integrated total amount of SO$_2$ for the S21-3D dataset. The red triangle marks the location of the volcano Sarychev Peak. **(c)** latitudinally integrated total amount of SO$_2$ for the S21-3D input dataset. **(d)** longitudinally integrated total amount of SO$_2$ for the S21-3D input dataset.

3 Results and discussion

3.1 Temporal and spatial evolution of volcanic SO$_2$

The difference in vertical the vertical SO2 distribution between M16 and the S21 datasets are retained after interpolation onto the rather course model grid (see Fig. S1). The S21 datasets show that half of the SO2 was injected to pressure levels below <150 hPa, and almost all SO2 was injected to the stratosphere, whereas M16 injected a large portion of the SO2 into the UT. The injected volcanic SO$_2$ profiles in the three simulations result in a large difference in SO$_2$ lifetime. Figure 2 shows the increase in global SO$_2$ load in the atmosphere following the June 2009 eruptions of the Sarychev peak. The volcanic SO$_2$ from M16 and S21-1D was injected on the 15 and the 16 of June with a total of 1.2 Tg for the M16 and 1.09 Tg for the S21-1D dataset. The S21-3D injected the SO$_2$ on the 19 of June with a total mass of 1.09 Tg. The global volcanic SO$_2$ levels for the M16 simulation (Fig. 2 black line) drop to levels below the simulations with S21-1D and S21-3D (orange and purple lines) by the beginning of July, regardless of the 0.11 Tg larger injected SO$_2$ mass in M16. The more rapid removal occurs since a large fraction of SO$_2$ in M16 is injected at altitudes below the tropopause, where the SO$_2$ is subject to the rapid wet chemistry
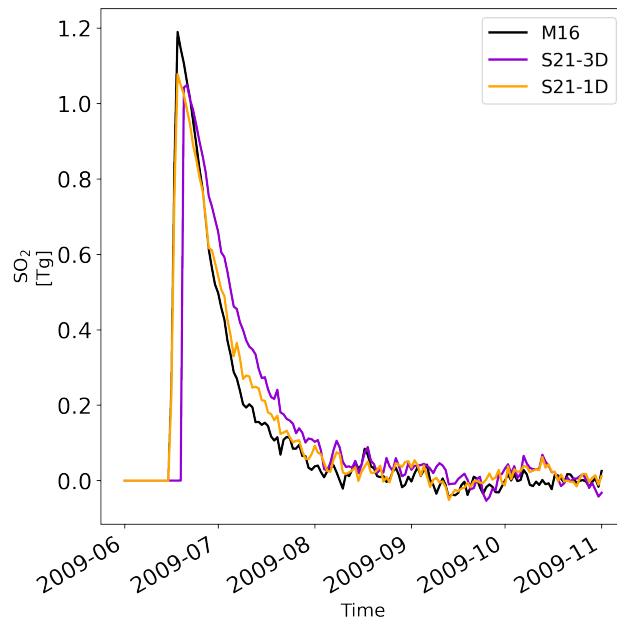
Figure 2. Global evolution of volcanic SO_2 in the M16, S21-1D and S21-3D simulations. To isolate the volcanic SO_2 we have subtracted the SO_2 levels in the No-Volc simulation from the other 3 simulations.

of the troposphere, causing the SO_2 to be removed more quickly compared to the S21-1D and S21-3D datasets (Fig. 3). In the S21-1D and S21-3D simulations, more than 95% of the total SO_2 mass was injected into the stratosphere whereas only 75% of the SO_2 was injected into the stratosphere in the M16 simulation.

The time evolution of the vertical distribution of the SO_2 concentration is shown in Fig. 3. The volcanic SO_2 is seen at 6 different times, 5 (a), 12 (b), 19 (c), 26 (d), 33 (e), and 40 (f) days after the volcanic eruption on the 15 of June. Both the stratospheric SO_2 mass (solid lines) and the total atmospheric (tropospheric + stratospheric) SO_2 mass (dashed lines) are shown. Fig. 3a shows SO_2 profiles for the first date where all the SO_2 has been emitted in all simulations. It can be seen that even though the model resolution is coarser than the S21 input datasets, there is still a structure with high SO_2 concentrations in narrower layers than in M16. Moreover, a large fraction of the SO_2 mass at lower altitudes are located in the troposphere in the M16 simulation. This is seen in Fig. 3a where the dashed line deviates from the stratospheric mass (solid line). The tropospheric SO_2 is removed rapidly, shown by the difference between the dashed and solid line for the M16 simulation, where most tropospheric SO_2 was removed already 12 days after the eruption (Fig 3b). There is very little difference between the solid and dashed lines for the S21 simulations demonstrating that most of this SO_2 is injected into the stratosphere. Not only is a larger fraction of SO_2 in the S21 simulations located in the stratosphere, the stratospheric SO_2 is also located at a higher altitudes, i.e. deeper into the stratosphere. This leads to higher SO_2 concentrations in the S21 simulations, in particular between 100 and 200 hPa. Also the horizontal SO_2 distribution impact the lifetime of the SO_2. In M16, SO_2 is spread more towards the
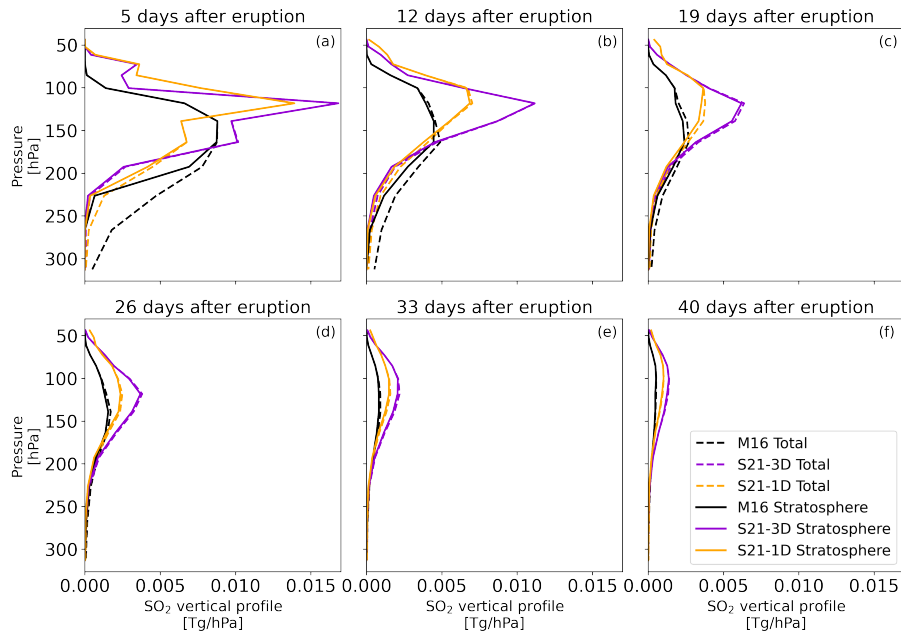
Figure 3. Vertical profile for for the global total volcanic SO_2 at 5 **(a)**, 12 **(b)**, 19 **(c)**, 26 **(d)**, 33 **(e)**, and 40 **(f)** days after the volcanic eruption on the 15 of June. The dashed lines represent the total amount of volcanic SO_2 in the atmosphere whereas the solid lines represent the total amount of volcanic SO_2 in the stratosphere. To isolate the volcanic SO_2 we have subtracted the SO_2 levels in the No-Volc simulation from the other 3 simulations.

subtropics (Fig. S2), where the tropopause is located at high altitudes, likely leading to more rapid cross-tropopause transport,

195   reducing the stratospheric SO_2 mass.

Even though the vertical SO_2 profiles for the two S21 datasets are rather similar after 5 days there is a pronounced difference in the maximum SO_2 concentrations up to one month after the simulation (Fig. 3). The difference between the two S21 simulations is most likely a result of differences in horizontal spread of the SO_2 in the two simulations, where SO_2 in S21-1D is transported more towards the subtropics leading to more cross-tropopause transport for S21-1D than S21-3D. This exemplifies

200   the sensitivity of the transport of the volcanic aerosol to air movement and weather patterns. Simulations of volcanic climate impact are often run with single column data of SO_2, where the volcanic injections are represented by vertical columns in single geographical (latitude $\times$ longitude) grid cell. Small errors/uncertainties in simulated air dynamics can result in vast differences in the geographical spread of the volcanic SO_2, leading to under- or overestimation of the aerosol lifetime and resulting climate cooling (e.g. Tilmes et al., 2023). Using the S21-3D dataset from satellite observations a few days after the eruption, where the

205   initial transport has already taken place, reduces the importance of the models' ability to correctly simulate the air movement at the time of the eruption.
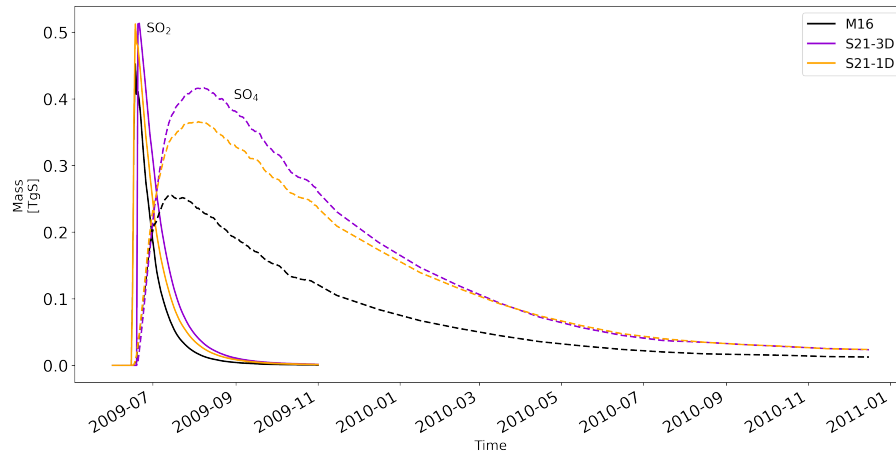
Figure 4. Stratospheric evolution of the amount of sulfur for SO_2 (solid lines) and SO_4 in the particle phase (dashed lines) over time. Daily values for both SO_2 and SO_4 til the end of October 2009, monthly values for SO_4 from November 2009 to December 2010. To isolate the volcanic SO_2 and SO_4 we have subtracted the SO_2 and SO_4 levels in the No-Volc simulation from the other 3 simulations.

3.2 Temporal and spatial evolution of volcanic SO_4

The injected SO_2 is converted to SO_4 over the first weeks after the injection. Figure 4 shows the resulting increase of SO_4 after the volcanic eruption together with the decreasing SO_2 in the stratosphere. The peak mass for SO_4 differs both in time and magnitude for the three simulations. In the M16 simulation SO_4 peaks in mid July, four weeks after the eruption. The S21-1D and S21-3D volcanic SO_4 peaks in August, approximately 8 weeks after the eruption.

The earlier peak date for M16 than S21-1D and S21-3D stems from the difference in their vertical profiles of SO_2, where S21-1D and S21-3D injected more SO_2 to higher altitudes. In M16, a larger fraction of the SO_2 is injected into the first few kilometers above the tropopause. Both the injected SO_2 and the resulting aerosol formed at these lower altitudes are transported out of the stratosphere more quickly than SO_2 and aerosol located at the higher altitudes, explaining the longer-lasting SO_4 and later peak for S21-1D and S21-3D. The SO_4 mass for S21-3D is substantially larger than for M16 already in July and remains higher throughout fall. In November the SO_4 mass is almost twice as high for S21-3D compared with M16 indicating a substantially larger volcanic climate impact in the S21-3D simulation. The SO_4 mass one and a half years after the eruption, December 2010, is still elevated for all three simulations. The S21 datasets have however an almost double amount of SO_4 mass at the end of 2010.

The large differences in volcanic sulfate aerosol loading over time is also visible in Fig. 5. The initial transport of the volcanic SO_2 results in different patterns in the SO_4 load between the datasets emitted as a single column and the S21-3D dataset. After this, the pattern of the SO_4 load is similar between the simulations but aerosol concentrations drop of more rapidly in the M16 simulation compared to the S21 datasets. The aerosol is mainly located at mid and high latitudes for all three simulations but there is substantial equatorward transport during the NH autumn and winter after the eruption.
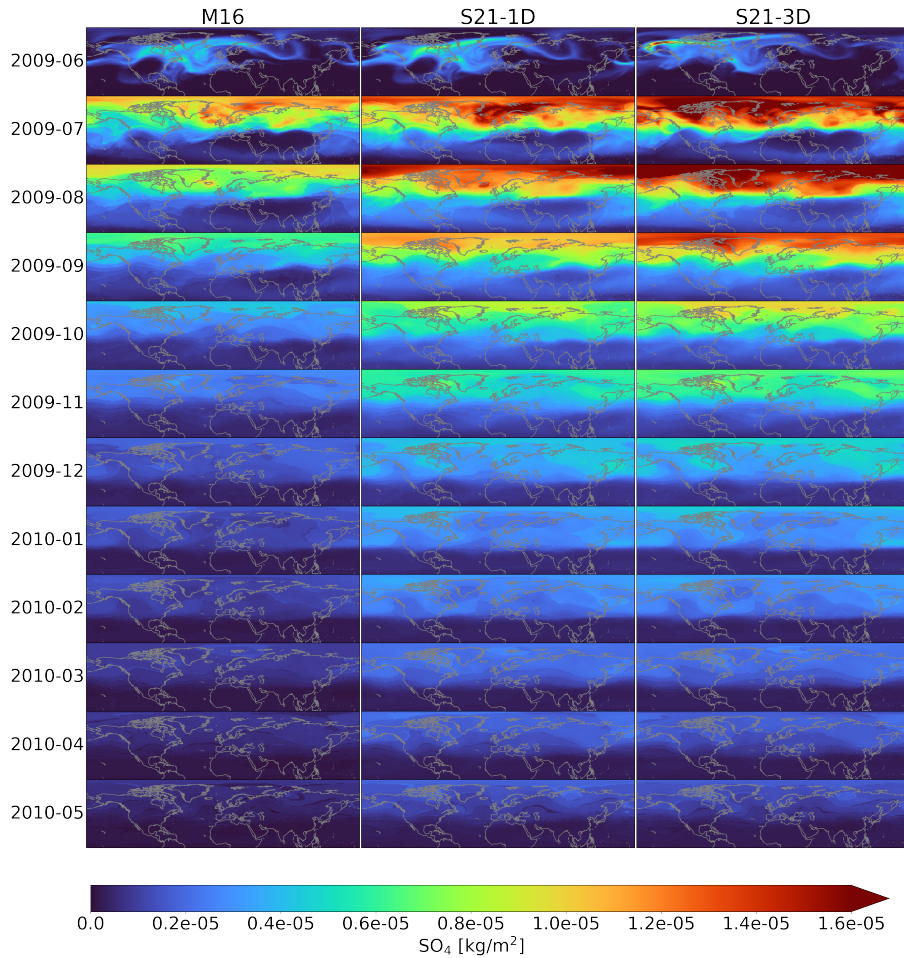
Figure 5. Monthly mean of stratospheric SO_4 in the NH during the first year post the volcanic eruption. To isolate the volcanic SO_4 we have subtracted the SO_4 levels in the No-Volc simulation from the other three simulations.

3.3 Comparison with CALIOP observations

Here we will compare the simulations with aerosol observations from the space-borne lidar CALIOP. This comparison is done for the aerosol extinction coefficient (Fig. 6) and AOD (Fig. 7). The first four columns in Fig. 6 represent simulations with the three datasets, M16, S21-1D, S21-3D, and CALIOP observations, where each row corresponds to monthly zonal mean values from June to November 2009. The fifth column in the figure shows the average aerosol extinction over all longitudes in the NH, i.e. extinction profiles. Since CALIOP is a polar orbiting satellite and only nighttime data from CALIOP is used in this study, there is missing data at high latitudes in the NH, in particular during the summer months. We have removed the data from the missing latitudes for all simulations to enable a direct comparison. We have also introduced a common tropopause mask to ensure that we compare data from the same latitudes and altitudes. All model simulations initially show lower extinction

235 values in the lowermost troposphere than the CALIOP observations. Averaging data in the proximity of the tropopause is complicated due to the strong concentration gradients in this altitude region. The satellite data contain a substantially higher vertical resolution of both the extinction data and tropopause altitude than the models do. The coarser resolution of the model results in less sharp concentration gradients in the tropopause region. Moreover, for the simulations, the division between the stratospheric and tropospheric data was done based on the maximum probability of the daily chemical tropopause which results

240 in that some of the lowest stratospheric data include influence from tropospheric air which will lower the extinction values. Above these lowest altitudes, the model simulations have similar extinction coefficients as the CALIOP observations. During July, the M16 profiles bear most resemblance to the CALIOP profiles but after this month, the profiles from the S21 simulations have values more similar to the CALIOP observations.

There are clear differences in the altitude-latitude distributions among the three simulations, where the S21 simulations show

245 higher extinction coefficients in the northern midlatitude LMS. Aerosol, in all simulations, spread to the tropics, but not to as high altitudes in the M16 as in the S21 simulations. This is expected due to the generally lower injection altitudes for the simulations with the M16 SO_2 dataset. The simulations predict lower extinction coefficients at the lowest kilometers of the northern midlatitudes and larger volcanic influence at higher altitudes. CALIOP shows the highest extinction coefficients at low altitudes, which is expected due to the higher pressure there. Furthermore, CALIOP shows that almost all aerosol remained

250 below 20 km altitude. Thus, it did not reach the upper branch of the BD circulation. Even though there are some differences between the three simulations and the CALIOP observations, the general patterns are however similar; The Sarychev eruption i) influenced mainly the midlatitudes, ii) was almost isolated within the NH, and iii) did not enter the deep BD branch.

The extinction coefficients for the simulations and observations start to attain similar values and gradients at most altitudes in August, following the initial phase of SO_2 transformation and particle formation (Jun-Jul), with the M16 showing the

255 lowest extinction coefficients. The S21 simulations continue to agree with observations in the following two months, whereas M16 starts to deviate more from the observations and show lower extinction coefficients than both observations and the S21 simulations. This pattern is most pronounced in the LMS, illustrating the influence of outflow from the stratosphere which leads to the lower AODs for M16 than for the S21 observations.

The resulting stratospheric AOD from the extinction profiles is shown in Fig. 7. The S21-1D simulation shows the best

260 agreement with CALIOP at almost all times. The S21-3D simulation peaks at higher values than CALIOP, while M16 display an increase in stratospheric AOD after the Sarychev eruption which is approximately 60% of that seen in CALIOP. The climate effects of stratospheric aerosol is not only dependent on the SO_4 mass but also on where in the size distribution the SO_4 is placed since particles of different sizes reflect different amounts of solar radiation (Laakso et al., 2022; Tilmes et al., 2023). We investigated this by calculating the average stratospheric aerosol effective radius (r_e) over time for all simulations 8a. The

265 initial response during the first few weeks after the eruption is a decrease in r_e, followed by an increase in r_e over the next months. The decrease and increase is largest in S21-3D and smallest in M16. The NoVolc simulation display a decrease over time since there is particle shrinkage after the Kasatochi eruption that occurred in August 2008.

To investigate the impact of the size distribution changes on the AOD we have divided the stratospheric AOD with the total stratospheric SO_4 mass (see Fig. 8b). This quantity illustrates whether the amount of light reflected per SO_4 mass vary
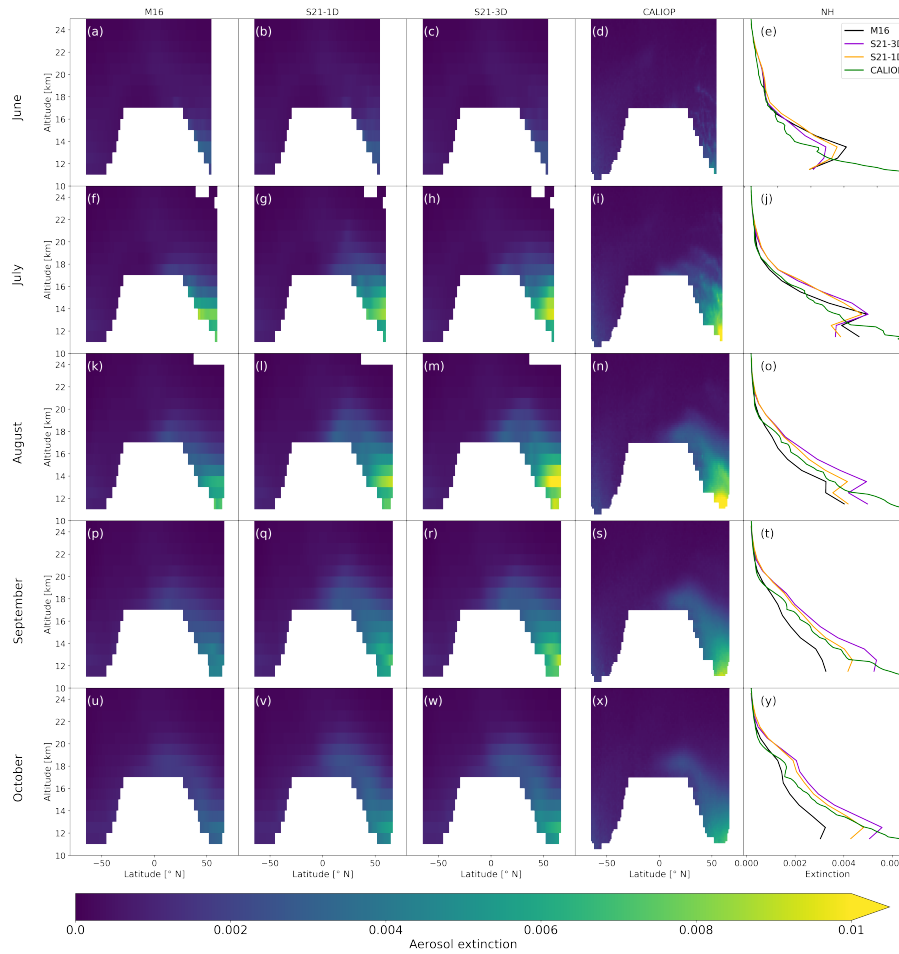
Figure 6. Zonal monthly mean stratospheric evolution of the aerosol extinction coefficient for the three simulations and satellite observations from CALIOP. The first three columns show the simulations, (M16, S21-1D, and S21-3D), and the fourth column represents the CALIOP observations. The fifth column shows the average vertical aerosol extinction profiles in the NH for both simulations and the observations. The rows correspond to different months, starting from June to November 2009. The white areas are excluded values located in the troposphere, and missing latitudes in CALIOP. Note that the simulations have a wavelength of 550 nm whereas CALIOP observations have a wavelength of 532 nm.

between the simulations. When the eruption occurs the AOD/SO_4 ratio decreases for all three volcanic simulations, with the largest decrease in the S21-3D simulation. Hence, the higher AOD values in the S21-3D simulation cannot be explained by a greater efficiency in light reflection for the SO_4 mass, pointing out cross tropopause transport as the major cause of difference in AOD among the simulations.
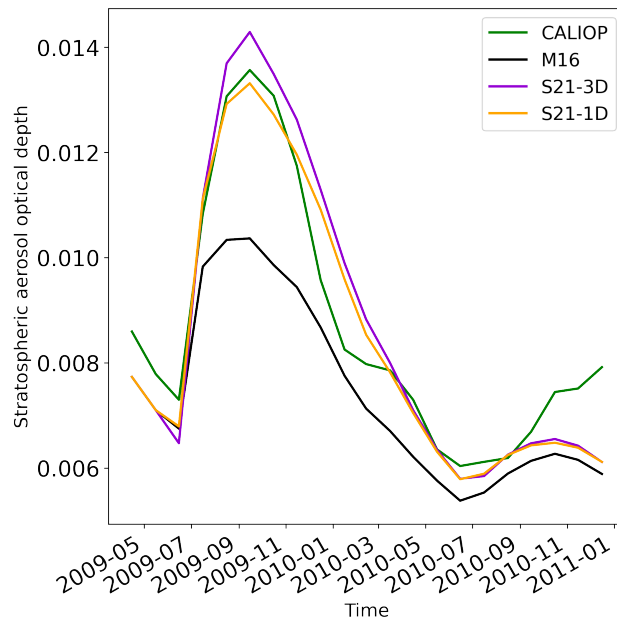
Figure 7. Global mean stratospheric Aerosol optical depth (AOD) for the three simulations M16, S21-3D, and S21-1D, compared with observations by CALIOP. Note that the simulations show AOD at 550 nm whereas CALIOP observations provide AODs at a wavelength of 532 nm.

3.4 Radiative forcing - comparison of simulations

275   Finally, we will evaluate the extent of volcanic climate cooling estimated by the three simulations. Figure 9 shows the global clear sky volcanic effective radiative forcing for the simulations. The effective radiative forcing (ERF) was calculated using the method suggested by Ghan (2013) which has previously been used for calculations of volcanic forcing by Schmidt et al. (2018). The S21-3D simulation, run with SO_2 at high vertical and horizontal resolution, predicts the highest and longest impact on the global volcanic forcing. The datasets with only high vertical resolution but released in single column, S21-1D, follow the

280   curve of S21-3D closely but with slightly lower values. The dataset with low vertical resolution M16, has the weakest global clear sky volcanic forcing which disappears more rapidly compared to the other two simulations. The peak value for the M16 simulation is -0.36 W/m^2 in August, the peak value for S21-1D is -0.41 W/m^2 in July and the peak value for S21-3D is -0.52 W/m^2 in August. The long-term forcing differed more among the models. The forcing during the first year post eruption was more than twice as high for the S21-3D than for simulations with the models default dataset M16, i.e. -0.24 and -0.11 W/m^2,

285   respectively (Table 2). This large difference exemplifies the importance of the vertical placement of volcanic SO_2 injections in global climate models.
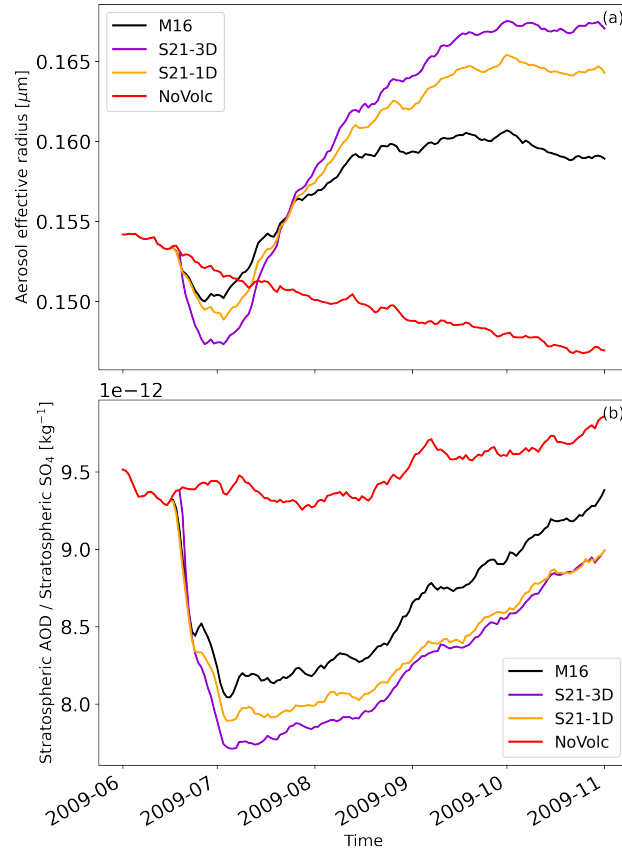
Figure 8. Global geometric mean stratospheric Aerosol effective radius (a) and stratospheric AOD divided by stratospheric SO$_4$ mass (b) for the four simulations M16, S21-3D, S21-1D and NoVolc.

Table 2. Global average volcanic effective radiative forcing for the 3 simulations for different time periods.

Volcanic ERF	2009	2010	June 2009 - May 2010
M16	-0.11	-0.018	-0.11
S21-3D	-0.19	-0.092	-0.24
S21-1D	-0.16	-0.061	-0.20
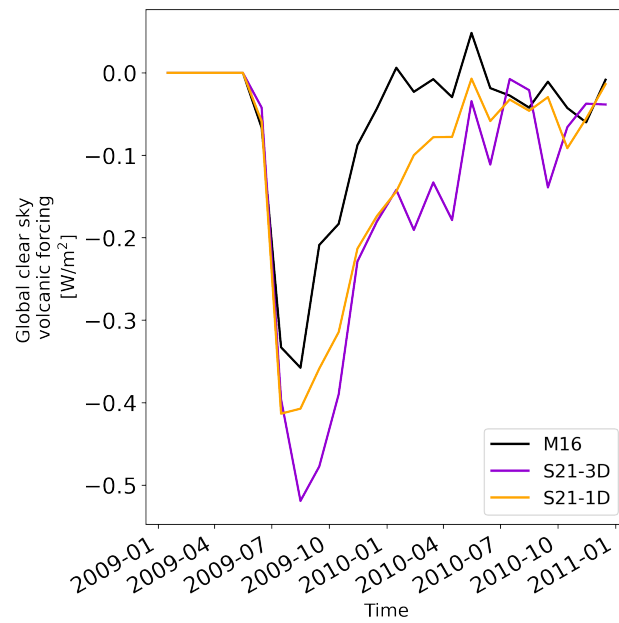
Figure 9. Global clear sky volcanic forcing from the Sarychev eruption for the three model simulations.

4 Conclusions

We have simulated the Sarychev eruptions' impact on the stratosphere and climate, using three different SO_2 injection profiles in WACCM (Whole Atmosphere Community Climate Model). The eruptions positioned SO_2 throughout the lowest stratosphere and upper troposphere, in an altitude range of 11-19 km, increasing the stratospheric aerosol load (AOD) by 100% in the months following the SO_2 injection. The overarching goal of this work was to investigate the influence of vertical SO_2 distributions on the stratospheric aerosol load and climate. To this end, we compared our simulations with high-vertical resolution observations from the satellite borne lidar instrument CALIOP.

WACCM simulations with the S21 SO_2 data sets captured the AOD well in the aftermath of the June 2009 Sarychev eruptions. Simulations with these datasets produced very similar temporal evolution in stratospheric AODs as observations from the satellite borne high-vertical resolution lidar instrument CALIOP. Furthermore, the simulated vertical distribution of the aerosol load, expressed by the aerosol extinction coefficients, agreed well with the CALIOP observations. On the other hand, simulations with the default volcanic injection dataset showed generally lower aerosol extinction coefficients and AODs.

Simulations with the S21-3D SO_2 dataset produced more than twice as strong volcanic forcing as the default dataset in WACCM. The global clear sky radiative forcing during the first year after eruption amounted to -0.24 (-0.11) W/m^2 for the high (low) resolution dataset. Although, holding 10% more SO_2, the default dataset induces far less climate cooling than the high resolution datasets do. These findings highlight the need to produce datasets of volcanic SO_2 injections to the stratosphere that precisely place the SO_2 at correct altitudes, especially when the eruptions reach the LMS. Moreover, the results indicate that our present understanding of volcanic climate cooling is in part limited by the SO_2 profiles and it is highly likely that not only the Sarychev eruptions' climate cooling is underestimated due to inaccurate assumptions on SO_2 profiles. Climate cooling of pre- and post-Sarychev eruptions may to varying degrees be under- or overestimated due to limited knowledge of the SO_2 vertical profiles. This highlights the need for further investigations of volcanic SO_2 profiles. Our study required high-vertical resolution satellite retrievals of aerosols which have until present only been accomplished by lidar. CALIOP provided us with such data from 2006 - 2023. This study highlights the usefulness of spaceborne lidar systems, the need for continuous atmospheric observations from such systems, and exemplifies the need for future space borne lidars.

Code and data availability. CESM is an open source model that is available to download through git, instructions are found here: https://www.cesm.ucar.edu/models/cesm2/download. The SO_2 input files for all simulations are available here: 10.5281/zenodo.11192344. Also monthly averaged model output from the simulations and monthly averaged CALIOP are available trough this link. CALIOP lidar data are open-access products available via https://search.earthdata.nasa.gov/search?fp=CALIPSO.

Author contributions. E.A. performed the model simulations with WACCM. E.A. did most of the data analysis with contributions from M.K.S and J.F.. J.F. compiled the aerosol extinction coefficient data from CALIOP. E.A. wrote the majority of the paper. M.K.S and J.F. wrote parts of the paper. All authors have contributed to the discussions regarding the manuscript.

Competing interests. The authors declare that they have no conflict of interest.

Acknowledgements. The computations and data handling were enabled by resources provided by the National Academic Infrastructure for
320   Supercomputing in Sweden (NAISS) and the Swedish National Infrastructure for Computing (SNIC) at Tetralith (project no 2023/22-1104,
2023/6-311, 2023/1-13 and 2024/23-95) partially funded by the Swedish Research Council through grant agreements no. 2022-06725 and
no. 2018-05973. The CALIOP Level 1b lidar data were produced by NASA Langley Research Center.

References

Andersson, S., Martinsson, B., Vernier, J., Friberg, J., Brenninkmeijer, C., Hermann, M., Velthoven, P., and Zahn, A.: Significant radiative impact of volcanic aerosol in the lowermost stratosphere, Nature communications, 6, 7692, https://doi.org/10.1038/ncomms8692, 2015.

Appenzeller, C., Holton, J. R., and Rosenlof, K. H.: Seasonal variation of mass transport across the tropopause, Journal of Geophysical Research: Atmospheres, 101, 15 071–15 078, https://doi.org/https://doi.org/10.1029/96JD00821, 1996.

Carboni, E., Grainger, R. G., Mather, T. A., Pyle, D. M., Thomas, G. E., Siddans, R., Smith, A. J. A., Dudhia, A., Koukouli, M. E., and Balis, D.: The vertical distribution of volcanic SO_2 plumes measured by IASI, Atmospheric Chemistry and Physics, 16, 4343–4367, https://doi.org/10.5194/acp-16-4343-2016, 2016.

Clarisse, L., Coheur, P.-F., Theys, N., Hurtmans, D., and Cl erbaux, C.: The 2011 Nabro eruption, a SO_2 plume height analysis using IASI measurements, Atmospheric Chemistry and Physics, 14, 3095–3111, https://doi.org/10.5194/acp-14-3095-2014, 2014.

Danabasoglu, G., Lamarque, J.-F., Bacmeister, J., Bailey, D., Duvivier, A., Edwards, J., Emmons, L., Fasullo, J., Garcia, R., Gettelman, A., Hannay, C., Holland, M., Large, W., Lauritzen, P., Lawrence, D., Lenaerts, J., Lindsay, K., Lipscomb, W., Mills, M., and Strand, W.: The Community Earth System Model version 2 (CESM2), Journal of Advances in Modeling Earth Systems, 12, https://doi.org/10.1029/2019MS001916, 2020.

Deshler, T.: A review of global stratospheric aerosol: Measurements, importance, life cycle, and local stratospheric aerosol, Atmospheric Research, 90, 223–232, https://doi.org/https://doi.org/10.1016/j.atmosres.2008.03.016, 17th International Conference on Nucleation and Atmospheric Aerosols, 2008.

Friberg, J., Martinsson, B. G., Andersson, S. M., and Sandvik, O. S.: Volcanic impact on the climate – the stratospheric aerosol load in the period 2006–2015, Atmospheric Chemistry and Physics, 18, 11 149–11 169, https://doi.org/10.5194/acp-18-11149-2018, 2018.

Friberg, J., Martinsson, B. G., and Sporre, M. K.: Short- and long-term stratospheric impact of smoke from the 2019–2020 Australian wildfires, Atmospheric Chemistry and Physics, 23, 12 557–12 570, https://doi.org/10.5194/acp-23-12557-2023, 2023.

Gettelman, A., Hoor, P., Pan, L. L., Randel, W. J., Hegglin, M. I., and Birner, T.: THE EXTRATROPICAL UPPER TROPOSPHERE AND LOWER STRATOSPHERE, Reviews of Geophysics, 49, https://doi.org/https://doi.org/10.1029/2011RG000355, 2011.

Gettelman, A., Mills, M., Kinnison, D., Garcia, R., Smith, A., Marsh, D., Tilmes, S., Vitt, F., Bardeen, C., Mcinerney, J., Liu, H., Solomon, S., Polvani, L., Emmons, L., Lamarque, J.-F., Richter, J., Glanville, A., Bacmeister, J., Phillips, A., and Randel, W.: The Whole Atmosphere Community Climate Model Version 6 (WACCM6), Journal of Geophysical Research: Atmospheres, 124, https://doi.org/10.1029/2019JD030943, 2019.

Ghan, S.: Technical Note: Estimating aerosol effects on cloud radiative forcing, Atmospheric Chemistry and Physics, 13, 9971–9974, https://doi.org/10.5194/acp-13-9971-2013, 2013.

Hansen, J. E., Sato, M., Simons, L., Nazarenko, L. S., Sangha, I., Kharecha, P., Zachos, J. C., von Schuckmann, K., Loeb, N. G., Osman, M. B., Jin, Q., Tselioudis, G., Jeong, E., Lacis, A., Ruedy, R., Russell, G., Cao, J., and Li, J.: Global warming in the pipeline, Oxford Open Climate Change, 3, kgad008, https://doi.org/10.1093/oxfclm/kgad008, 2023.

Haywood, J. M., Jones, A., Clarisse, L., Bourassa, A., Barnes, J., Telford, P., Bellouin, N., Boucher, O., Agnew, P., Clerbaux, C., Coheur, P., Degenstein, D., and Braesicke, P.: Observations of the eruption of the Sarychev volcano and simulations using the HadGEM2 climate model, Journal of Geophysical Research: Atmospheres, 115, https://doi.org/https://doi.org/10.1029/2010JD014447, 2010.

Höpfner, M., Boone, C. D., Funke, B., Glatthor, N., Gr abowski, U., Günther, A., Kellmann, S., Kiefer, M., Linden, A. a nd Lossow, S., Pumphrey, H. C., Read, W. G., Roiger, A., Stiller, G., Schlager, H., von Clarmann, T., and Wissmüller, K.: Sulfur dioxide

360   (SO$_2$) from MIPAS in the upper troposphere and low er stratosphere 2002–2012, Atmospheric Chemistry and Physics, 15, 7017–7037, https://doi.org/10.5194/acp-15-7017-2015, 2015.

IPCC: Climate Change 2021: The Physical Science Basis. Contribution of Working Group I to the Sixth Assessment Report of the Intergovernmental Panel on Climate Change, vol. In Press, Cambridge University Press, Cambridge, United Kingdom and New York, NY, USA, https://doi.org/10.1017/9781009157896, 2021.

365   Jäger, H. and Deshler, T.: Lidar backscatter to extinction, mass and area conversions for stratospheric aerosols based on midlatitude balloonborne size distribution measurements, Geophysical Research Letters, 29, 35–1–35–4, https://doi.org/https://doi.org/10.1029/2002GL015609, 2002.

Jäger, H. and Deshler, T.: Correction to "Lidar backscatter to extinction, mass and area conversions for stratospheric aerosols based on midlatitude balloonborne size distribution measurements", Geophysical Research Letters, 30,
370   https://doi.org/https://doi.org/10.1029/2003GL017189, 2003.

Kerminen, V. M. and Kulmala, M.: Analytical formulae connecting the "real" and the "apparent" nucleation rate and the nuclei number concentration for atmospheric nucleation events, Journal of Aerosol Science, 33, 609–622, https://doi.org/https://doi.org/10.1016/S0021-8502(01)00194-X, 2002.

Kremser, S., Thomason, L., Von Hobe, M., Hermann, M., Deshler, T., Timmreck, C., Toohey, M., Stenke, A., Schwarz, J., Weigel,
375   R., Fueglistaler, S., Prata, F., Vernier, J., Schlager, H., Barnes, J., Antuña-Marrero, J. C., Fairlie, T., Palm, M., Mahieu, E., and Meland, B.: Stratospheric aerosol - Observations, processes, and impact on climate, Reviews of Geophysics, 54, n/a–n/a, https://doi.org/10.1002/2015RG000511, 2016.

Laakso, A., Niemeier, U., Visioni, D., Tilmes, S., and Kokkola, H.: Dependency of the impacts of geoengineering on the stratospheric sulfur injection strategy – Part 1: Intercomparison of modal and sectional aerosol modules, Atmospheric Chemistry and Physics, 22, 93–118,
380   https://doi.org/10.5194/acp-22-93-2022, 2022.

Liu, X., Easter, R. C., Ghan, S. J., Zaveri, R., Rasch, P., Shi, X., Lamarque, J.-F., Gettelman, A., Morrison, H., Vitt, F., Conley, A., Park, S., Neale, R., Hannay, C., Ekman, A. M. L., Hess, P., Mahowald, N., Collins, W., Iacono, M. J., Bretherton, C. S., Flanner, M. G., and Mitchell, D.: Toward a minimal representation of aerosols in climate models: description and evaluation in the Community Atmosphere Model CAM5, Geoscientific Model Development, 5, 709–739, https://doi.org/10.5194/gmd-5-709-2012, 2012.

385   Liu, X., Ma, P.-L., Wang, H., Tilmes, S., Singh, B., Easter, R., Ghan, S., and Rasch, P.: Description and evaluation of a new four-mode version of the Modal Aerosol Module (MAM4) within version 5.3 of the Community Atmosphere Model, Geoscientific Model Development, 9, 505–522, https://doi.org/10.5194/gmd-9-505-2016, 2016.

Martinsson, B. G., Friberg, J., Sandvik, O. S., and Sporre, M. K.: Five-satellite-sensor study of the rapid decline of wildfire smoke in the stratosphere, Atmospheric Chemistry and Physics, 22, 3967–3984, https://doi.org/10.5194/acp-22-3967-2022, 2022.

390   Mills, M., Schmidt, A., Easter, R., Solomon, S., Kinnison, D., Ghan, S., Neely, R., Marsh, D., Conley, A., Bardeen, C., and Gettelman, A.: Global volcanic aerosol properties derived from emissions, 1990-2014, using CESM1(WACCM), Journal of Geophysical Research: Atmospheres, 121, https://doi.org/10.1002/2015JD024290, 2016.

Mills, M. J., Richter, J. H., Tilmes, S., Kravitz, B., MacMartin, D. G., Glanville, A. A., Tribbia, J. o. J., Lamarque, J.-F., Vitt, F., Schmidt, A., Gettelman, A., Hannay, C., Bacmeister, J. T., and Kinnison, D. E.: Radiative and Chemical Response to Interactive Strato-
395   spheric Sulfate Aerosols in Fully Coupled CESM1(WACCM), Journal of Geophysical Research: Atmospheres, 122, 13,061–13,078, https://doi.org/https://doi.org/10.1002/2017JD027006, 2017.

Myhre, G., Shindell, D., Bréon, F.-M., Collins, W., Fuglestvedt, J., Huang, J., Koch, D., Lamarque, J.-F., Lee, D., Mendoza, B., Naka-jima, T., Robock, A., Stephens, G., Takemura, T., and Zhang, H.: Anthropogenic and natural radiative forcing, in: Climate Change 2013: The Physical Science Basis. Contribution of Working Group I to the Fifth Assessment Report of the Intergovernmental Panel on Climate Change, edited by Stocker, T. F., Qin, D., Plattner, G.-K., Tignor, M., Allen, S. K., Boschung, J., Nauels, A., Xia, Y., Bex, V., and Midgley, P. M., p. 658–740, Cambridge University Press, Cambridge, United Kingdom and New York, NY, USA, https://doi.org/10.1017/CBO9781107415324.018, 2013.

Neely, R. R. and Schmidt, A.: VolcanEESM: Global volcanic sulphur dioxide (SO2) emissions database from 1850 to present, 2016.

Robock, A.: Volcanic Eruptions and Climate, Reviews of Geophysics, 38, 191, https://doi.org/10.1029/1998RG000054, 2000.

Rybin, A., Chibisova, M., Webley, P., Steensen, T., Izbekov, P., Neal, C., and Realmuto, V.: Satellite and ground observations of the June 2009 eruption of Sarychev Peak volcano, Matua Island, Central Kuriles, Bulletin of Volcanology, 73, 1377 – 1392, https://doi.org/10.1007/s00445-011-0481-0, 2011.

Sandvik, O., Friberg, J., Sporre, M. K., and Martinsson, B.: Methodology to obtain highly resolved SO_2 vertical profiles for representation of volcanic emissions in climate models, Atmospheric Measurement Techniques, 14, 7153–7165, https://doi.org/https://doi.org/10.5194/amt-14-7153-2021, 2021.

Schmidt, A., Mills, M., Ghan, S., Gregory, J., Allan, R., Andrews, T., Bardeen, C., Conley, A., Forster, P., Gettelman, A., Portmann, R., Solomon, S., and Toon, O.: Volcanic Radiative Forcing From 1979 to 2015, Journal of Geophysical Research: Atmospheres, 123, https://doi.org/10.1029/2018JD028776, 2018.

Sigl, M., Winstrup, M., McConnell, J. R., Welten, K. C., Plunkett, G., Ludlow, F., Büntgen, U., Caffee, M., Chellman, N., Dahl-Jensen, D., Fischer, H., Kipfstuhl, S., Kostick, C., Maselli, O. J., Mekhaldi, F., Mulvaney, R., Muscheler, R., Pasteris, D. R., Pilcher, J. R., Salzer, M., Schüpbach, S., Steffensen, J. P., Vinther, B. M., and Woodruff, T. E.: Timing and climate forcing of volcanic eruptions for the past 2,500 years, Nature, 523, 543–549, https://doi.org/10.1038/nature14565, 2015.

Solomon, S., Daniel, J. S., Neely, R. R., Vernier, J.-P., Dutton, E. G., and Thomason, L. W.: The Persistently Variable "Background" Strato-spheric Aerosol Layer and Global Climate Change, Science, 333, 866–870, https://doi.org/10.1126/science.1206027, 2011.

Tilmes, S., Mills, M. J., Zhu, Y., Bardeen, C. G., Vitt, F., Yu, P., Fillmore, D., Liu, X., Toon, B., and Deshler, T.: Description and performance of a sectional aerosol microphysical model in the Community Earth System Model (CESM2), Geoscientific Model Development, 16, 2023.

Timmreck, C., Mann, G., Aquila, V., Hommel, R., Lee, L., Schmidt, A., Brühl, C., Carn, S., Chin, M., Dhomse, S., Diehl, T., English, J., Mills, M., Neely, R., Sheng, J.-X., Toohey, M., and Weisenstein, D.: The Interactive Stratospheric Aerosol Model Intercomparison Project (ISA-MIP): Motivation and experimental design, Geoscientific Model Development, 11, 2581–2608, https://doi.org/10.5194/gmd-11-2581-2018, 2018.

Vehkamäki, H., Kulmala, M., Napari, I., Lehtinen, K. E. J., Timmreck, C., Noppel, M., and Laaksonen, A.: An improved parameterization for sulfuric acid–water nucleation rates for tropospheric and stratospheric conditions, Journal of Geophysical Research: Atmospheres, 107, AAC 3–1–AAC 3–10, https://doi.org/https://doi.org/10.1029/2002JD002184, 2002.

Vehkamäki, H., Kulmala, M., Napari, I., Lehtinen, K. E. J., Timmreck, C., Noppel, M., and Laaksonen, A.: Correction to "An improved parameterization for sulfuric acid/water nucleation rates for tropospheric and stratospheric conditions", Journal of Geophysical Research: Atmospheres, 118, 9330–9330, https://doi.org/https://doi.org/10.1002/jgrd.50603, 2013.

Vernier, J., Thomason, L., Pommereau, J.-P., Bourassa, A., Pelon, J., Garnier, A., Hauchecorne, A., Blanot, L., Trepte, C., Degenstein, D., and Vargas, F.: Major influence of tropical volcanic eruptions on the stratospheric aerosol layer during the last decade, GEOPHYSICAL RESEARCH LETTERS, 38, https://doi.org/10.1029/2011GL047563, 2011.